J. Appl. Comput. Mech., 11(4) (2025) 1009-1021
DOI: 10.22055/jacm.2024.47786.4793

ISSN: 2383-4536
jacm.scu.ac.ir

Shahid Chamran University of Ahvaz

Journal of Applied and Computational Mechanics

Research Paper

Experimental Investigation of the Relationship Between Cavitation Acoustic Waves and Erosion Threshold with a Novel Piezoelectric Configuration

Amir Nasseroleslami[1], Ali Sarreshtehdari[1], Mohamad Saeed Seif[2], Ali Asghar Ebrahimi Valmoozi[3]

[1] Faculty of Mechanical Engineering, Shahrood University of Technology, Shahrood, 3619995161, Iran,
Email: Amir.eslami@live.com (A.N.); Email: sarreshtehdari@shahroodut.ac.ir (A.S.)

[2] Department of Mechanical Engineering, Sharif University of Technology, Tehran, 1458889694, Iran, Email: seif@sharif.edu

[3] Department of Mechanical Engineering, Imam Hussein University, Tehran, 1698715461, Iran, Email: aa.ebrahimivalmoozi@ihu.ac.ir

Received August 21 2024; Revised November 01 2024; Accepted for publication December 20 2024.
Corresponding author: A. Sarreshtehdari (sarreshtehdari@shahroodut.ac.ir)

Abstract. An optimal solution for the rapid prediction of cavitation erosion is to identify parameters that can be quickly detected and have a logical and effective correlation with erosion. One of these important parameters is the Sound Pressure Level (SPL) generated by cavitation. In the process of calculating the eroded surface area, a uniform special paint is applied to the sample plate using a film applicator to enhance the visibility of surface erosion. In the designed channel for this study, four bluff bodies are utilized as the best method to accelerate the onset of cavitation. Piezoelectric sensors are employed to record signals generated by cavitation, and for the first time, the optimal arrangement of these sensors has been established using CFD analysis. In this study, the threshold for the eroded surface area can be detected in the shortest possible time using a strategy that identifies the SPL pattern resulting from cavitation. Another advantage of this method is that since the piezoelectric sensors are connected to the area where erosion needs to be examined (or its corresponding region), the relationship obtained between SPL and the eroded surface area is independent of the geometry and dimensions of the water tunnel. Therefore, the established relationship remains valid even with changes in the experimental environment.

Keywords: Erosion threshold, Sound pressure level, Semi-cylindrical bluff body, Piezoelectric, Vapor volume fraction, K23 cavitation tunnel.

1. Introduction

In recent years, various experimental and numerical studies have investigated the impact of mass transfer models for identifying different flow characteristics and parameters leading to sudden pressure drops, cavitation, and its collapse. Three types of flow geometries are most commonly used as they can effectively represent different cavitation models. These geometries are: (1) internal flows and liquid flow through converging nozzles, (2) flow over hydrofoils, and (3) flow around geometric obstacles. Since flow around geometric obstacles can generate more extensive cavitation and be more erosive, the focus will be on studies related to the third type of flow geometry.

Detecting cavitation erosion effectively is essential for preventing costly repairs and ensuring operational efficiency. Traditional inspection methods, such as visual assessments and ultrasonic testing, have their limitations, particularly in terms of accuracy and the ability to provide real-time data. Consequently, there is a growing interest in developing advanced detection techniques that can offer more precise, non-destructive evaluations of cavitation damage. Cavitation erosion detection has advanced significantly with the introduction of electronic tools, particularly piezoelectric sensors. These sensors leverage the unique properties of piezoelectric materials, which generate an electrical charge in response to mechanical stress. This capability makes them highly effective for monitoring the onset and severity of cavitation erosion in real time. Overall, incorporating piezoelectric sensors into cavitation erosion detection represents a significant advancement in predictive maintenance. Their ability to provide real-time, sensitive, and non-invasive monitoring positions them as a valuable tool for industries relying on hydraulic machinery. Continued research and development in this area promise to enhance the effectiveness of cavitation management strategies, ultimately improving equipment longevity and operational efficiency. In conclusion, it should be noted that there are many methods for detecting cavitation, one of the most optimal being the use of piezoelectric sensors to capture the acoustic signals resulting from cavitation, which has been utilized in this experiment. There are many methods for detecting cavitation, among which one of the most effective approaches is using piezoelectrics to capture the acoustic signals generated by cavitation. The

Published online: December 27 2024

correlation obtained from acoustic signals and the level of erosion can facilitate the detection of the extent of erosion. In the following sections, the studies conducted on the generation of cavitation, methods for its detection, and the correlation between cavitation and erosion will be discussed.

Around bluff bodies, vortexes with low pressure and high sensitivity to cavitation generation flow in an irregular and random manner. Research conducted by Scaler et al. [1] shows that installing a small bluff body on a hydrofoil causes severe localized erosion, where bubbles collapse in a narrow region due to the bluff body. The cavitation characteristics around a bluff body can be highly dependent on the shape of the body. Kumar et al. observed a reduction in vortex shedding frequency in their experimental and numerical studies. They were the first to conduct a detailed analysis of cavitation flow structures in the shear layer and behind a cylinder [2, 3]. Additionally, numerous studies indicate that cavitation affects the noise generated by cylindrical obstacles [4].

Aside from cylindrical geometries, studies have also been conducted on other shapes. Brandner et al. [5] experimentally investigated cavitation flow on a sphere with a Reynolds number of 1.5×10^6 and a cavitation number ranging from 0.36 to 1. According to this study, the boundary layer at cavity separation remains stable for various cavitation numbers. One common application of bluff bodies is the study of vortex shedding that occurs behind them [6, 7]. Yamagata et al. [8], in an experimental study, compared the peak sound spectra at different angles of attack for semi-circular and circular cylinders. The results showed that the peak sound spectrum of the semi-circular cylinder is smaller than that of the circular cylinder, with the value reaching a minimum at zero angle of attack. This is due to the smaller oscillatory lift force on the semi-circular cylinder compared to the circular cylinder.

Cavitation is known for the damage it can cause to hydrodynamic structures and is therefore considered a condition to be avoided. However, bluff bodies are used to accelerate the erosion process in tests of material damage and various coatings. Ghahramani et al. [9] investigated cavitation flow around a semi-cylinder both experimentally and numerically. They also examined various cavitation flow characteristics resulting from the cylinder's effect. Based on their previous studies, they employed a semi-cylindrical obstacle to induce greater erosion [9]. In an experimental study, Scaler et al. placed four obstacles at the inlet of a hydrofoil to increase flow erosion. They found that the semi-cylindrical obstacle is suitable for generating repeatable pitting on samples in a short period [10]. Over the years, many experimental techniques have been developed to study cavitating flows. High-speed visualization, due to its exceptional temporal resolution, is the most popular technique for investigating cavitation evolution. This method helps capture details of transient flow behavior, as demonstrated in the recent study by Ghahramani et al. [9]. They employed a transport equation based on the finite mass model, which has shown satisfactory results compared to computational studies in previous research [11-13]. To complement their study, they used experimental testing to measure the erosion pattern resulting from cavitation with colorimetric tests. It was shown that the color test method can significantly reduce the measurement period while producing a similar erosion pattern compared to previous studies [14].

1.1. Studies on the acoustics of cavitation erosion and their correlation

The Sound Pressure Level (SPL) of cavitation is the sound generated during cavitation progression, primarily resulting from bubble collapse. Under specific conditions, micro-jets and micro-shocks can be produced during bubble collapse. The impact of micro-jets and micro-shocks on material surfaces is strong enough to damage the material structure, leading to erosion. Research on SPL caused by cavitation is limited. Park et al. [15] experimentally studied the ultrasonic degradation of endocrine-disrupting compounds in seawater and brine. Lawrence explored aspects of cavitation and physical acoustics relevant to sonochemistry. He found that at similar acoustic intensities, cavitation bubbles grow for approximately 25 microseconds at low frequencies (20 kHz), while bubbles at higher frequencies (1 MHz) grow for only 0.5 microseconds. These significant differences in bubble growth result in smaller bubbles at higher frequencies, leading to less intense collapses [16]. Usta et al. [17] investigated the acoustics and cavitation erosion in marine propellers using water jet techniques. In their study, the cavitation number is defined as:

$$\sigma = \frac{P_{upstream}}{P_{downstream}} = \frac{P_{chamber}}{P_{water\ jet}} \tag{1}$$

They found that as the cavitation number decreases, both erosion and acoustic intensity increase. However, the erosion rate as follows:

$$\text{Erosion rate} = \frac{weight\ loss(gr)}{test\ duration\ (min)} \tag{2}$$

may not necessarily increase. Han et al. [18] examined the contribution and impact of acoustic shocks from micro-jets or shock waves but did not address the relationship or pattern between acoustic levels and the extent of erosion. Homa [19] compared various cavitation models by studying the flow over a Clark-Y airfoil. According to this research, selecting the optimal cavitation model requires evaluating several parameters, including the angle of attack, variations in lift and drag with time, and not just relying on the flow pattern. Therefore, a single, specific cavitation model cannot be recommended for numerical analyses of cavitation flow simulations, as changes in geometry and flow components can affect model selection.

Researchers have studied the correlation between cavitation acoustics and cavitation erosion for over 50 years. Notable works include those by Varga et al. [20] in 1969, Ramamurthy et al. [21] in 1979, and Di et al. [22] in 1982. More recent studies by Bal et al. [23] and Rathod [24] have investigated cavitation detection using piezoelectric sensors and hydrophones. However, a precise pattern and relationship between noise levels and the extent of erosion have not yet been established.

As a summary, this section discusses the need for a new method and the challenges associated with existing techniques for detecting cavitation. Need for a New Method:

- Cavitation erosion can cause significant damage to equipment in industries like aerospace, marine engineering, and hydraulic systems, leading to costly repairs and downtime. Timely detection is essential for maintaining equipment integrity and performance.
- Existing methods often struggle to provide timely and accurate assessments. Many rely on subjective visual inspections or advanced imaging techniques that are expensive and time-consuming. This can delay necessary maintenance and increase the risk of catastrophic failures.

Shortcomings of Existing Techniques:

- Subjectivity and Inconsistency: Traditional visual inspections can be highly subjective, leading to inconsistencies in assessments of erosion severity. This variability can result in missed early signs of damage.
- Sensitivity to Operational Conditions: Many acoustic monitoring methods lack the specificity needed to differentiate between cavitation-related sounds and other noise sources, leading to potential false positives or negatives.

- Geometry Dependence: Some techniques are sensitive to the specific geometry and setup of the experimental environment, limiting their applicability across different conditions. This can hinder the transferability of results to real-world applications.
- Delayed Detection: Existing methods may only provide post-event analysis, making it difficult to act quickly to mitigate further damage.

The method used in this experiment:

- Rapid Prediction: A novel method focuses on quickly correlating Sound Pressure Level (SPL) with erosion thresholds, enabling faster assessments compared to traditional techniques. In this study, the rapid detection of SPL, as opposed to calculating the extent of erosion through experimental and numerical analyses, is utilized. SPL data obtained from piezoelectric sensors are stored, and the relationship with the erosion threshold level is then calculated, which represents the main finding of this research.
- Independence from Geometry: By establishing a relationship between SPL and eroded surface area that is independent of specific geometries, your method offers broader applicability across various operational conditions.

For the first time, this study also explains the optimal arrangement of piezoelectrics for recording signals generated from the cavitation process using CFD analysis. The experimental techniques employed in this study include using a semi-cylindrical body as the most effective obstacle for accelerating cavitation generation at the test section, applying a specific color for rapid identification of the erosion pattern on sample plates, and using a Film Applicator as the best tool for achieving a uniform color and thin coating for cavitation erosion detection.

2. Experimental Setup

According to the technical specifications of the K23 cavitation tunnel, the maximum speed in the test section reaches 3.6 m/s. At this speed, the pressure does not drop below the vapor pressure of the fluid, so there is no potential for bubble formation and cavitation. To achieve the desired speed and induce cavitation, a converging-diverging channel was designed based on head loss calculations and the pump performance curve. The schematic of this channel is shown in Fig. 1.

Based on the research conducted in [4-8], cavitation-induced erosion increases after the fluid flow passes over a semi-cylindrical obstacle. Therefore, a semi-cylindrical obstacle was used in this experiment to accelerate erosion on the sample plate. The semi-circular obstacle is installed at the beginning of the flow entry into the test section, with the sample plate placed afterward. To investigate the dimensions of the sample plate, the optimal arrangement of piezoelectrics, and the minimum flow speed required in the test section to induce cavitation, CFD analysis was used. This simulation was performed using Star CCM+, and the simulation process will be explained in detail. Star CCM+ is a powerful computational fluid dynamics (CFD) software that excels in multiphysics simulation. In terms of cavitation, Star CCM+ provides specialized modeling tools to accurately simulate this phenomenon, which occurs when vapor bubbles form in a liquid due to pressure drops, subsequently collapsing and causing potential damage to surfaces. The software includes advanced turbulence models and multiphase flow capabilities that enable users to analyze cavitation dynamics in detail.

As explained in the introduction, to investigate the relationship between the acoustic data from cavitation, stored by piezoelectrics, and the level of erosion, a sample plate coated with paint and placed after the bluff body is used. Before applying the paint, the sample plate is acid-washed, and its surface roughness is measured with a Mitutoyo SurfTest device, as shown in Fig. 2. In the study conducted, an R_a value of 1.55 ± 0.1 μm was reported, which is considered desirable.

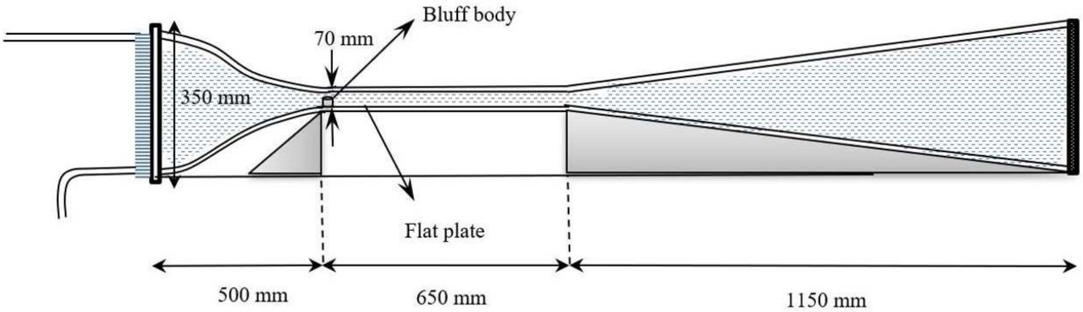

Fig. 1. Side view of the schematic of the converging-diverging channel installed in the test section of the K23 cavitation tunnel.

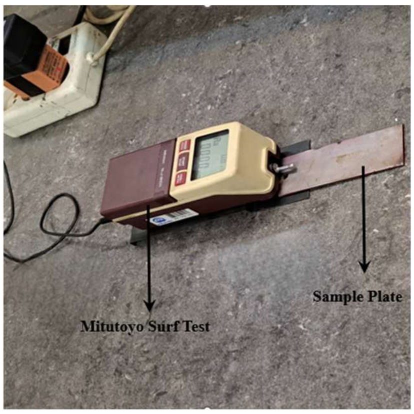

Fig. 2. Surface roughness measurement of the sample plate using the Mitutoyo SurfTest device.

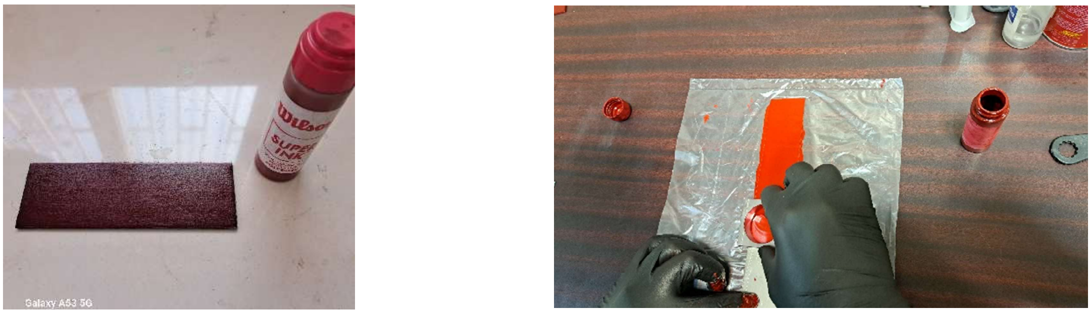

(a) (b)

Fig. 3. (a) Wilson Super Ink and the sample plate, (b) Use of the Film Applicator to apply paint to the sample plate.

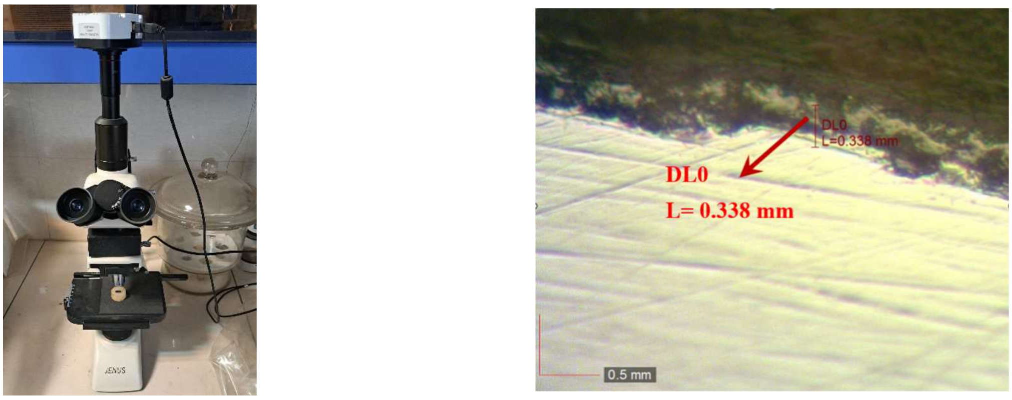

(a) (b)

Fig. 4. (a) Measurement of paint thickness using the JENUS optical microscope, (b) Paint thickness of 0.338 mm as measured by the microscope.

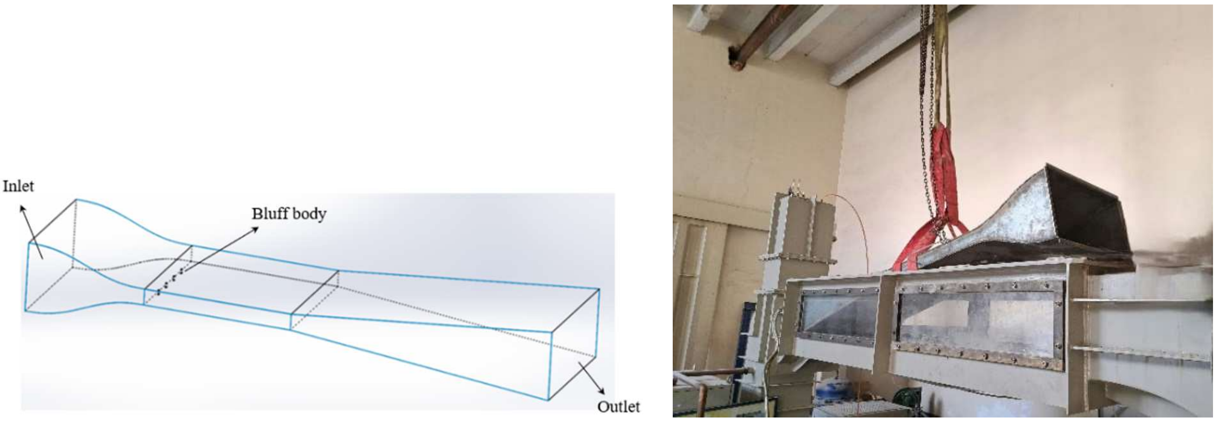

(a) (b)

Fig. 5. (a) Schematic of the channel designed for installation in the test section, (b) Installation of the channel in the test section of the K23 cavitation tunnel.

Various methods for applying paint to the plate were tested, including spraying with different tools and injection with a syringe. None of these methods were successful. Spraying with different tools led to excessive paint adhesion to the sample plate, while syringe injection, contrary to the claim by Jahangir et al. [14], resulted in excessive paint thickness. Ultimately, a Film Applicator was used to achieve a uniform, thin coating, which proved to be the most effective tool for this purpose (Fig. 3). In addition to determining the thickness with the Film Applicator, a JENUS optical microscope is also used to measure the paint thickness on a portion of the sample plate prepared using the Cold Mounting method (Fig. 4). The sample plate has been divided into several sections. Three of these sections were examined separately using an optical microscope, and the color uniformity was confirmed with a precision of 0.01 mm

Figure 5 shows the geometry of the equipment designed in SolidWorks for the simulation. In this model, all surfaces except for the Inlet and Outlet are considered as Walls.

Considering that the maximum inlet speed to the test section is 3.6 m/s (according to the K23 Manual [25]), the inlet speeds for the test section were set between 2 m/s and 3.5 m/s. The boundary condition at the outlet is pressure, which is set to the operating pressure of the flow according to the experimental test conditions. Since a no-slip condition is applied to the geometries of the tunnel channel and the semi-cylindrical bluff body, a wall boundary condition is used for these geometries. The settings listed in Table 1 were selected to ensure the accurate simulation of this problem in STAR-CCM+ software.

To evaluate grid independence, a point is selected 55 mm downstream of the bluff body, in a region where vapor volume fraction can occur. The number of grid cells is varied across six stages, and as shown in Fig. 6, the pressure variation becomes negligible after 8.2 million cells. Therefore, this cell count (8.2 million) is deemed sufficient for solving the problem.

Table 1. Settings for solving the problem.

Explanations	Settings
The flow is three-dimensional	Three Dimensional
The flow is transient	Implicit Unsteady
The flow is turbulent	Turbulent
Reduction in computational volume – optimal accuracy in cavitation simulation [26-28]	RANS
Superiority of this Turbulence Model Compared to Other RANS Models [28]	Realisable K Epsilon Two Layer
Convergence, improved accuracy, and faster computation – optimal accuracy – increased computational speed	Segregated Flow
Using wall functions to improve the accuracy of simulation results	Two-Layer All y+ Wall Treatment
Three-phase nature of the problem	Multiphase
For modeling cavitation and phase interactions of the problem	Multiphase Interaction
Gravity affects the flow	Gravity

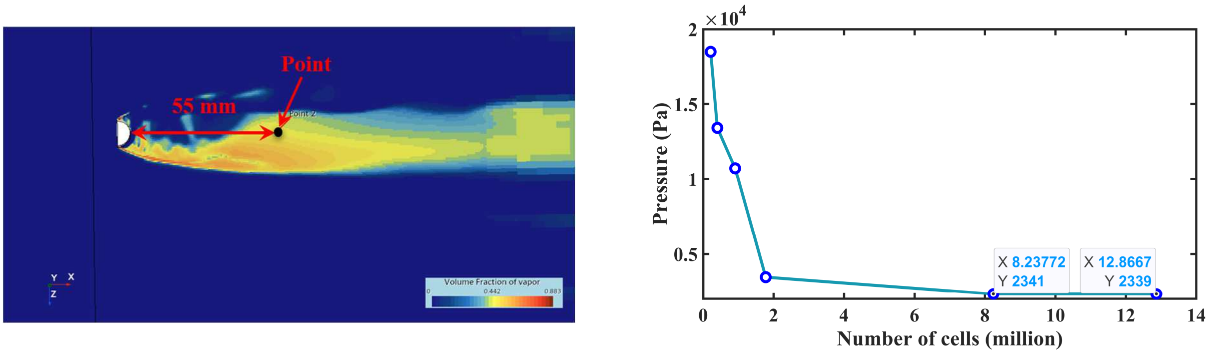

(a) (b)

Fig. 6. (a) Placement of a point downstream of the bluff body for the grid independence study, (b) Grid Independence Study.

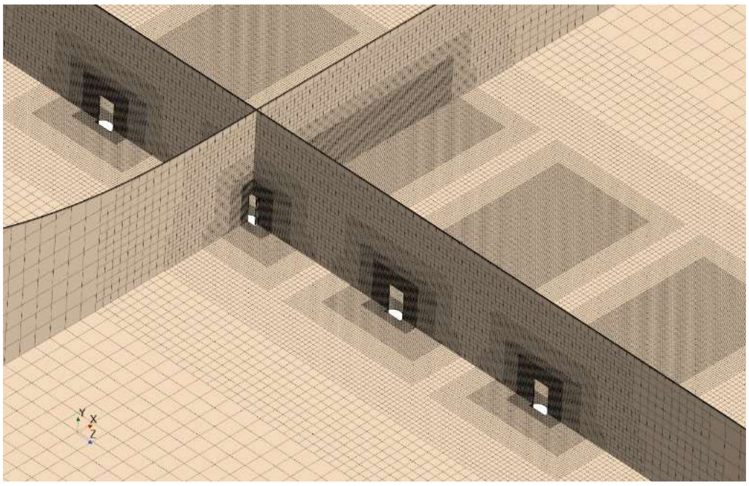

Fig. 7. Grid generation at the intersection of planes with a semi-cylindrical bluff body.

A view of the generated mesh is shown in Fig. 7, which utilized three meshing methods: Surface Remesher, Trimmed Mesher, and Prism Layer Mesher.

Among the three models provided by Star CCM+ for cavitation modeling, the Schnerr-Sauer model has been used. According to the software guide, the Homogeneous Relaxation model is intended for detecting the vapor phase (cavitation) in instantaneous boiling, which occurs due to sudden pressure changes [29]. However, the Schnerr-Sauer model, based on a simplified version of the Full Rayleigh–Plesset model developed by researchers, is used for cavitation modeling and provides high accuracy in simulating this phenomenon [28, 30]. The points discussed below present additional reasons for choosing this model.

- The Schnerr-Sauer model is specifically designed to capture the dynamics of cavitation and vapor bubble behavior in incompressible flows. Its ability to simulate the growth and collapse of bubbles makes it suitable for applications where cavitation plays a critical role.
- This model incorporates key physical mechanisms, such as the nucleation of vapor bubbles and their interaction with the surrounding liquid. It can effectively represent the phase change between liquid and vapor, which is essential in accurately simulating cavitation phenomena.
- This model incorporates key physical mechanisms, such as the nucleation of vapor bubbles and their interaction with the surrounding liquid. It can effectively represent the phase change between liquid and vapor, which is essential in accurately simulating cavitation phenomena.
- Compared to more complex models, the Schnerr-Sauer model strikes a balance between accuracy and computational efficiency. This is particularly important for simulations where a large number of iterations or long time scales are involved.

3. Results

3.1. CFD results and the placement of the piezoelectric

Simulations were conducted at inlet velocities of 2 m/s, 2.5 m/s, 3 m/s, and 3.5 m/s. Figure 8 shows the vapor volume fraction at 2 m/s and 2.5 m/s after 1 second. At 2 m/s, no vapor volume fraction is observed. Therefore, the minimum inlet velocity required to induce cavitation in the test section must be 2.5 m/s.

Figure 9 shows the effective vapor volume fraction resulting from this velocity over a length of 10 cm. 2 cm at the end of the sample plate is allocated for connections, so the length of the sample plate will be 12 cm. In this experiment, to avoid errors in recording acoustic cavitation data (pressure attenuation of cavitation bubbles passing through the sample plate and adhesive [31]) and to prevent errors in calculating the eroded area, the piezoelectric sensors are not attached to the sample plate. Instead, the piezoelectric sensors are placed in locations where the flow pattern resembles that on the sample plate. Additionally, as shown in Fig. 9, three piezoelectric sensors with a diameter of 27 mm will be used to cover the cavitation region. The simulation is transient, and the formation of the vapor phase is time-dependent. The range of vapor volume fraction variation remains constant after a certain amount of numerical solution, which can be predicted by observing the residuals of the vapor volume fraction equations. The residuals of these equations were monitored at all velocities, and it was found that after 2500 iterations (0.5 s), the fluctuation range of the vapor volume fraction remained constant, thus a reliable solution time of 1 second was chosen.

In this experiment, because the flow pattern changes after each piezoelectric sensor due to irregularities in the mounting and sealing, the three piezoelectric sensors are not aligned in a single row. Each sensor is positioned behind a bluff body, and the distance from the main bluff body is determined through CFD analysis. This distance must be such that the flow patterns behind each sensor do not interfere with one another. CFD analysis revealed that the bluff bodies must be spaced 95 mm apart to ensure that the regions of pressure and velocity variation behind them do not overlap at any velocity. For example, Fig. 10 (a) shows the velocity contour at an inlet speed of 3.5 m/s, and Fig. 10 (b) presents the vapor volume fraction formed after the bluff bodies, which are similar to each other.

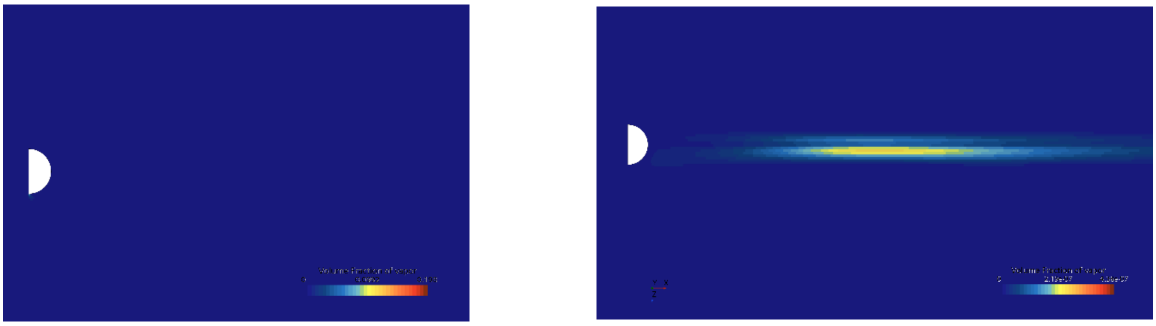

(a) (b)

Fig. 8. (a) Top view of the vapor volume fraction at 2 m/s after 1 second, (b) Top view of the vapor volume fraction at 2.5 m/s after 1 second.

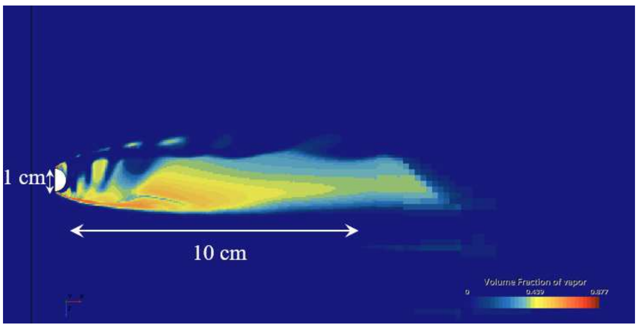

Fig. 9. Top view of the vapor volume fraction at 3.5 m/s after 1 second.

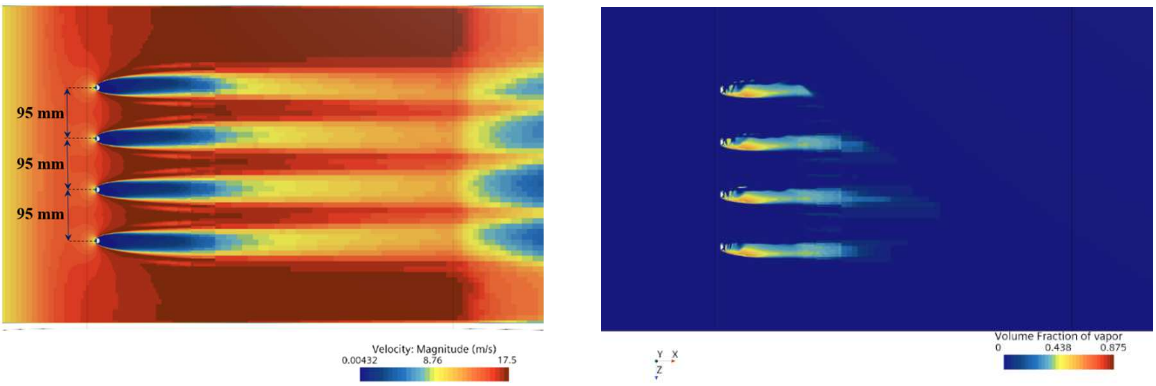

(a) (b)

Fig. 10. (a) Top view of the velocity contour at an inlet speed of 3.5 m/s after 1 second, (b) Top view of the vapor volume fraction at an inlet speed of 3.5 m/s after 1 second.

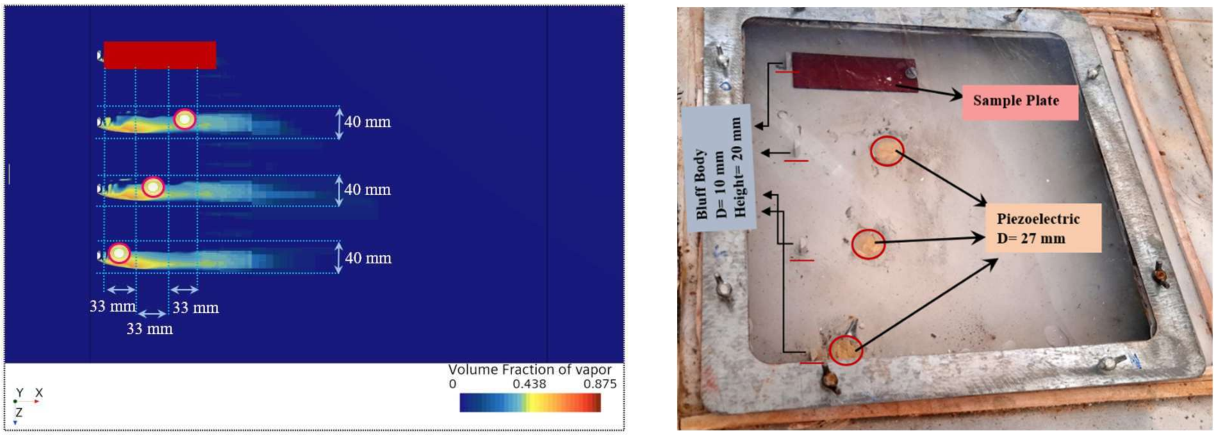

(a) (b)

Fig. 11. (a) Schematic of the optimal arrangement of the piezoelectric sensors and the sample plate based on CFD analysis, (b) Installation of the piezoelectric sensors, sample plate, and bluff body on the channel, based on CFD analysis.

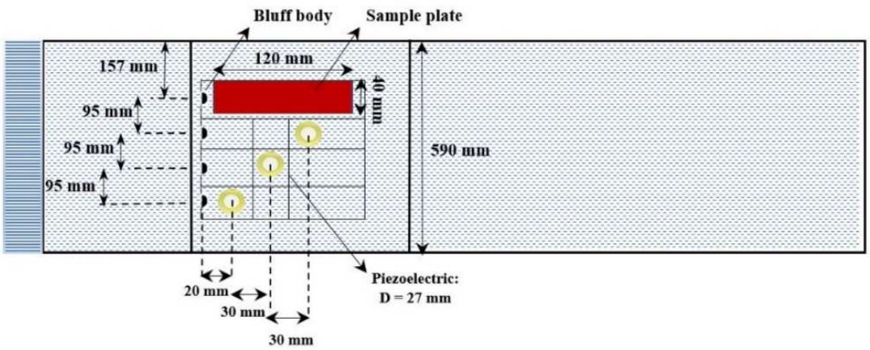

Fig. 12. Top view of the schematic layout of the piezoelectric sensors in the designed equipment for use in the test section of the K23 cavitation tunnel.

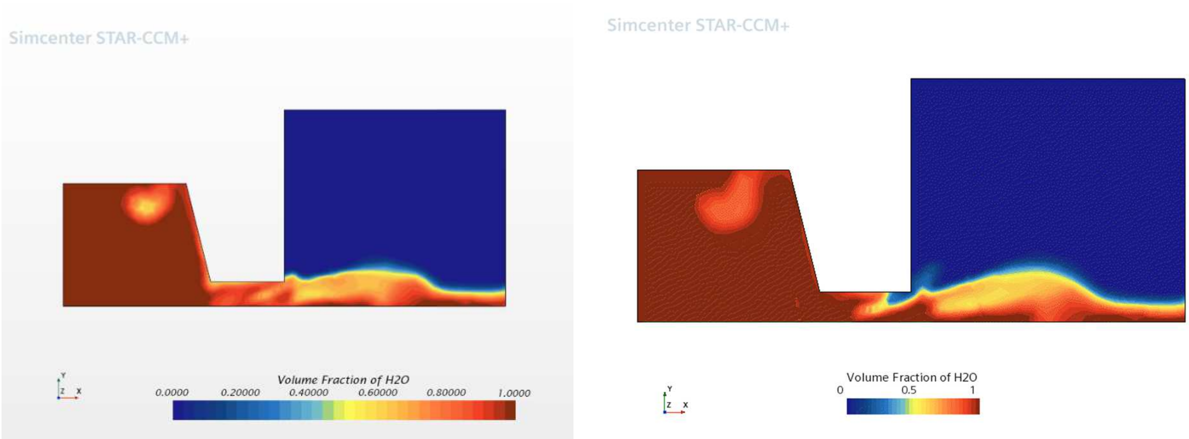

(a) (b)

Fig. 13. (a) Water volume fraction at 5 seconds from numerical analysis, (b) Water volume fraction at 5 seconds from the tutorial solution.

Based on Fig. 9, the cavitation region extends 10 cm in the longitudinal direction and 4 cm in the transverse direction, and the arrangement of the piezoelectric sensors must cover this area. Figure 11 (a) shows the optimal arrangement of the piezoelectric sensors and the sample plate, while Fig. 11 (b) shows the equipment installed in the test section of the channel.

Figure 12 shows a top view schematic of the channel dimensions with the piezoelectric sensors and bluff bodies installed. In this experiment, a GL820 data logger was used to record signals generated by cavitation. The voltage variation range observed during the tests was between +1 and -1 volts. To reduce noise, an earth wire was connected to the device. The data acquisition frequency was set to 10 Hz. The goal of this paper is not to investigate the collapse of cavitation bubbles, but rather to examine the erosion caused by cavitation. The collapse of cavitation bubbles can occur at frequencies up to 100 kHz [32].

To validate the CFD results, a gravity-driven flow simulation in two interconnected chambers was performed and compared with the STAR-CCM+ tutorial [29]. While it may seem unrelated to cavitation at first glance, understanding gravity-driven flows can provide insights into how fluids behave under different conditions, including the formation of vapor bubbles and cavitation phenomena. In many systems, the interplay between gravity, pressure changes, and flow dynamics can significantly influence cavitation behavior. Therefore, modeling these flows is crucial for a comprehensive analysis of fluid behavior in engineering applications.

Referring to Fig. 13, the left chamber, which is filled with water, allows the fluid to transfer to the right chamber. The boundary conditions are such that all boundaries are rigid except for the upper horizontal surface on the left, which is maintained at a fixed pressure (atmospheric pressure). Due to gravity, water flows into the right chamber. As the air compresses, the pressure in the right chamber increases until the fluid comes to rest and hydrostatic equilibrium is achieved. This problem involves multiphase flow with two fluids, water and air. Due to the turbulence in the flow, the k-epsilon turbulence model is used, and the gravitational force acts in the -y direction. The simulation runs for 5 seconds, and the water volume fraction at 5 seconds is shown in Fig. 13, demonstrating good agreement with the water volume fraction at 5 seconds in the tutorial.

3.2. Comparison of the eroded surface and the signals recorded from the piezoelectric sensor

The experiment was conducted at four inlet velocities: 2.5 m/s, 3 m/s, and 3.5 m/s, with test durations of 40 minutes, 50 minutes, 60 minutes, and 70 minutes, respectively. According to Fig. 11 (a), the sample plate needs to be divided into three sections to evaluate the correlation between the signals recorded from the sensors and the erosion on the plate. Accordingly, the sample plate is divided into three sections: A1, A2, and A3 (see Fig. 15), each assessed with its corresponding sensor. A total of 36 series of signals are obtained from all the experiments. After each test, the sample plate is removed from the channel for examination of the eroded surface. For this purpose, the plate is placed under a specific illumination and photographed, and the threshold is determined using ImageJ. In this study, a uniform color layer is utilized on the sample plate to facilitate the detection of erosion. The erosion threshold is defined as the point at which erosion becomes visible at all tested speeds in each of the three sections of the sample plate (A1, A2, A3); however, in this case, the area of the eroded section cannot be measured. Therefore, after this stage and upon completion of all tests, a photograph of the sample plate is taken, and the image is imported into ImageJ. Initial adjustments are made in the software (including converting the image type to 8-bit and specifying the plate size). The image is then processed in the threshold section. Based on the changes that occur within the byte range of the image (0-255) due to wear, the area of the created threshold is determined.

Additionally, the signals extracted from the cavitation process are converted to pressure using Eq. (3) [33], and the resulting pressures are then converted to Sound Pressure Level (SPL) using Eq. (4) [34]:

$$V = \frac{d_{33}Ft}{\varepsilon_r \varepsilon_0 A} \to P = \frac{V\varepsilon_r \varepsilon_0}{d_{33}t} \tag{3}$$

The piezoelectric sensor used in this experiment is a ceramic disc type with a diameter of 27 mm. The relevant values used in Eq. (3) are listed in Table 2.

$$SPL = 20log_{10}\frac{P_{rms}}{P_{ref}} \tag{4}$$

$$P_{ref} = 20\mu Pa,\ P_{rms} = \text{root mean square pressure}$$

This experiment was conducted over different durations. Depending on the length of the experiment, each piezoelectric sensor records a set of signals. For example, when the experiment lasts for 40 minutes, each piezoelectric sensor records 24,000 signals at each speed. Thus, during the 40-minute duration of the experiment, the piezoelectric sensors will send a total of 216,000 signals to the data logger for three different speeds.

When a set of signals $V_1, V_2, V_3, \dots$ is extracted from a piezoelectric sensor at a specific speed and time, the root mean square (RMS) is calculated using the following formula:

$$V_{RMS} = \sqrt{\frac{V_1^2 + V_2^2 + V_3^2 + \cdots}{n}} \tag{5}$$

where n is the number of signals.

From the 36 series of signals obtained from the experiment, a group is selected to examine changes in the amplitude and pulse of the signal (e.g., the group corresponding to the 2.5 m/s test, 40 minutes on surface A1). Analysis of the acoustic power spectrum for this test reveals that, over the test duration, the average amplitude or pulse of the signal remains constant with no significant changes (see Fig. 14 (a)). The constancy of the maximum and minimum signal amplitude and the uniformity of the average indicate that the duration of the test does not affect the signal amplitude. Therefore, it is sufficient to identify the minimum time required to establish an erosion threshold on the sample plate. During this time, the relationship between SPL and the eroded surface can be investigated to determine the correct placement of the piezoelectric sensor and to formulate this relationship. Additionally, Fig. 14 (b) shows the changes in SPL with increasing time at different speeds. This plot indicates that changes in SPL with time are minimal across various sensors, with a maximum variation of 0.7%. Noise reduction was achieved by connecting a ground wire to the data logger and using shielded cables for data transmission from the piezoelectric sensors to the data logger, which helped protect the signals. Proper installation of the piezoelectric sensors, ensuring they are not connected to the body, as well as the design and fabrication of the nozzle for the channel based on a relationship aimed at increasing velocity and preventing boundary layer separation in water tunnels [35], were key factors contributing to the accuracy of the experimental results. In this experiment, the erosion threshold is defined based on the visibility of erosion in all three sections of the sample plate (A1, A2, A3). In some references that utilize color, this duration (40 minutes) is also considered the threshold for cavitation erosion [14]. Thus, this time frame is used to examine the relationship between SPL and the eroded surface.

Figure 15 (a) shows the threshold area of the eroded surface (at different inlet velocities with a duration of 40 minutes) and compares it with the SPL measurements for the three corresponding sections of the sample plate. Finally, Fig. 15 (b) shows that, for all sensors and at different velocities over a duration of 40 minutes, there is a simultaneous increase and decrease in both SPL and the percentage of the eroded surface. This agreement and alignment confirm the correct placement of the piezoelectric sensors. Table 3 shows the SPL and the threshold area of the eroded surface at 40 minutes for various velocities.

Table 2. Specifications of the piezoelectric ceramic material [36].

Item	Symbol (Unit)	P-7
Piezoelectric constant	d_{33} (10^{-12} m/V)	410
Relative dielectric constant	ε_r	2100
Vacuum permittivity	ε_0 (Farad/m)	8.854×10^{-12}
Thickness	t (mm)	0.3

Table 3. Percentage of the threshold area of the eroded surface and SPL on the sample plate at different velocities with a duration of 40 minutes.

Inlet fluid velocity to the channel	Sensor number and its corresponding section	Spl (dB)	Percentage of the threshold area of the eroded surface (%)
	A251 (Sensor 1, A1)	121.1	26
2.5 m/s	A252 (Sensor 2, A2)	125	35
	A253 (Sensor 3, A3)	118.2	12
	A301 (Sensor 1, A1)	125.2	37
3 m/s	A302 (Sensor 2, A2)	122.3	31
	A303 (Sensor 3, A3)	119	13
	A351 (Sensor 1, A1)	125.8	41
3.5 m/s	A352 (Sensor 2, A2)	123	34
	A353 (Sensor 3, A3)	120.1	18

3.3. Signal analysis and the relationship between SPL and the threshold area of the eroded surface

After the optimal placement of the sensors, the signals received from them are analyzed at various velocities and times. When averaging the SPL from the sensors at each velocity and plotting the results, as shown in Fig. 16 the variation in the average plot with increasing time is minimal, suggesting that time does not significantly affect SPL. Another observation from the plots in Fig. 16 is that sensor behavior varies with increasing velocity. For the first and third sensors, SPL increases with velocity, while for the second sensor, SPL initially decreases and then increases. Notably, the average plot (the average SPL of the sensors at each velocity) increases as velocity increases.

Figure 17 (a) attempts to plot the SPL of the sensors at different velocities and times on a single graph for comparison. The first three points correspond to Sensor 1, the next three points to Sensor 2, and the final three points to Sensor 3. At all times, a significant difference in SPL is evident between Sensor 3 and Sensors 1 and 2. However, the average SPL of Sensors 1 and 2 appears similar, which will be examined more closely in Fig. 17 (b). This comparison will illustrate the impact of erosion on the sample plate. It will be determined which areas of the surface experience the most erosion if the average SPL is considered based on velocity.

Figure 17 (b) shows that at all velocities, the greatest effect of cavitation occurs in range 1, followed by range 2, and most significantly in range 3. This is further confirmed by Fig. 18, which illustrates the volumetric fraction of vapor generated after the bluff body. As seen in Fig. 11 (a), when the effective vapor volume created after the bluff body is divided into three sections, the largest vapor volume is observed in sections 1, 2, and 3, respectively. However, when considering each velocity independently, it is not possible to determine the order of the areas with the most erosion, as the SPL distribution among the three areas may vary with each velocity. Therefore, when tests are conducted over a specific velocity range, using the average SPL based on velocity is necessary to identify the order of the areas on the sample plate that experience the most erosion.

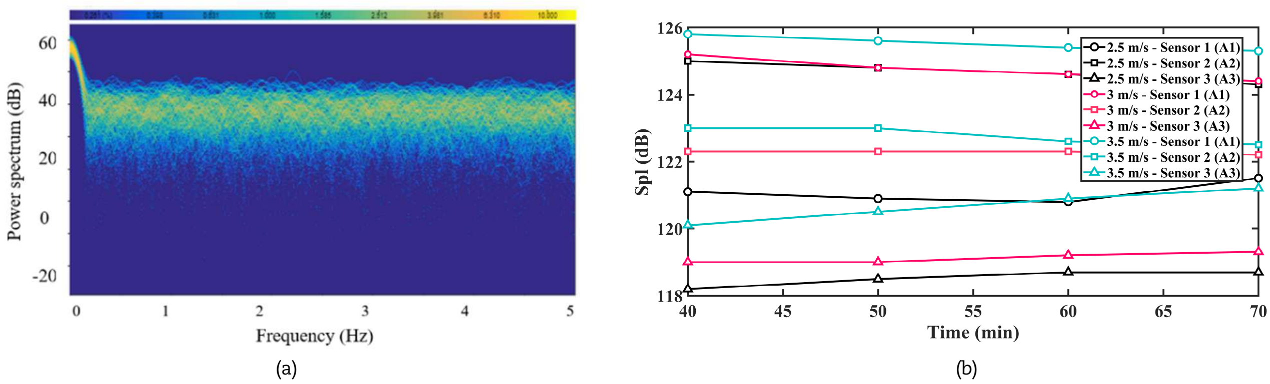

Fig. 14. (a) Acoustic power spectrum (dB), (b) Changes in SPL with increasing time at velocities of 2.5 m/s, 3 m/s, and 3.5 m/s.

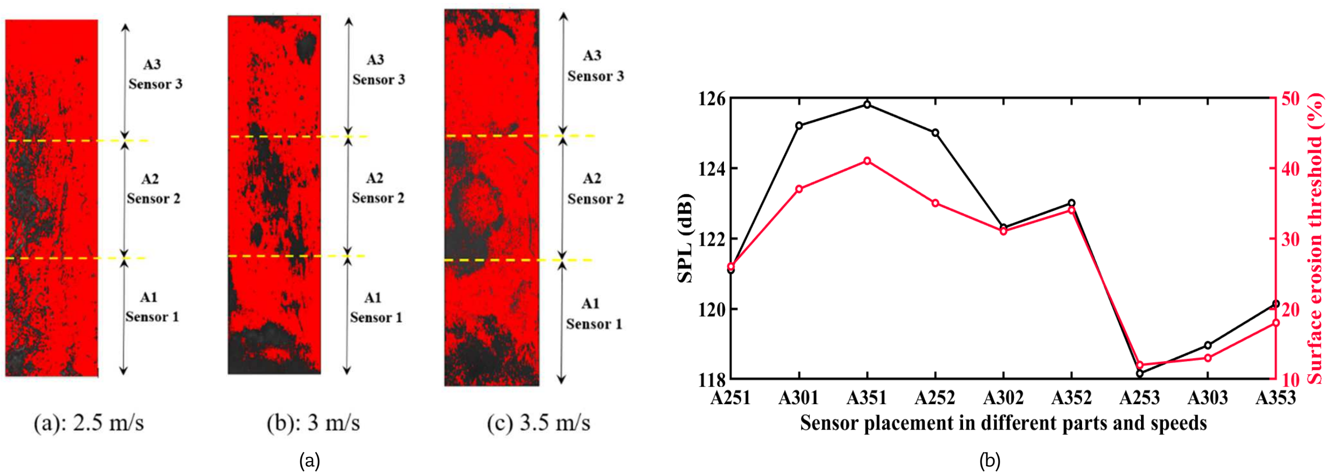

Fig. 15. (a) Threshold area of the eroded surface at inlet velocities of 2.5 m/s, 3 m/s, and 3.5 m/s with a duration of 40 minutes, (b) Alignment of SPL and the threshold area of the eroded surface at 40 minutes for various velocities.

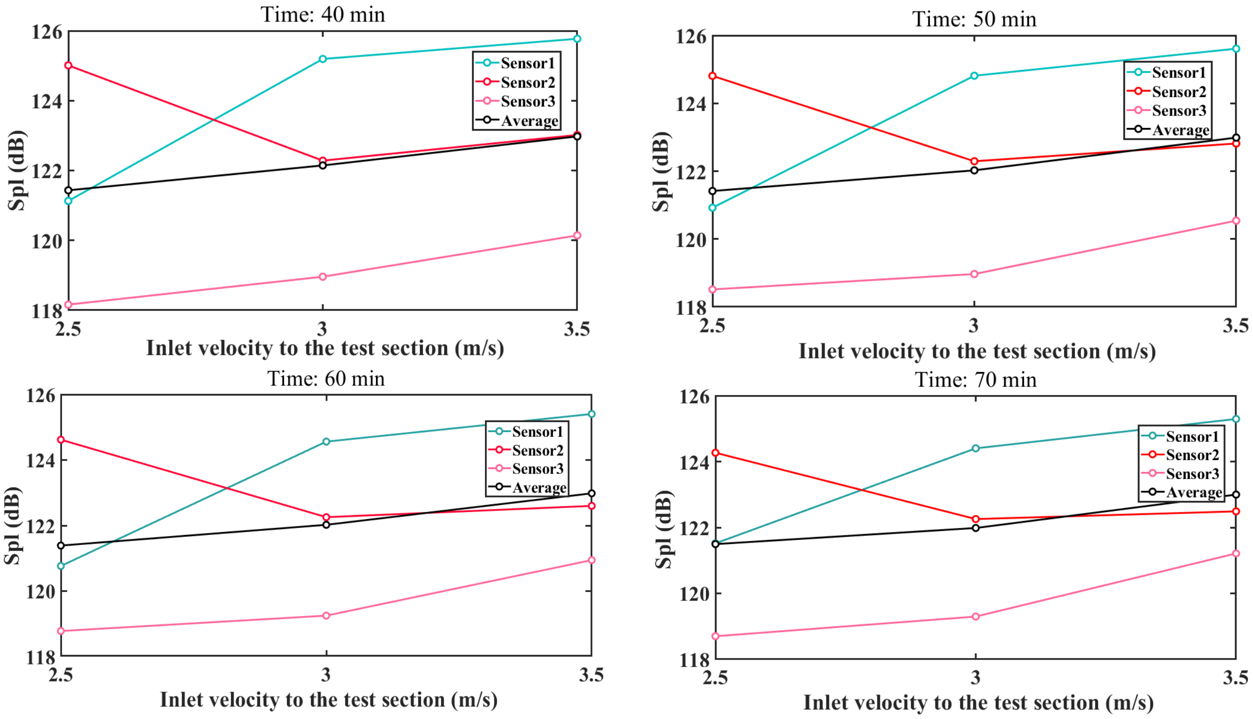

Fig. 16. Changes in sensor SPL with increasing velocity at different times.

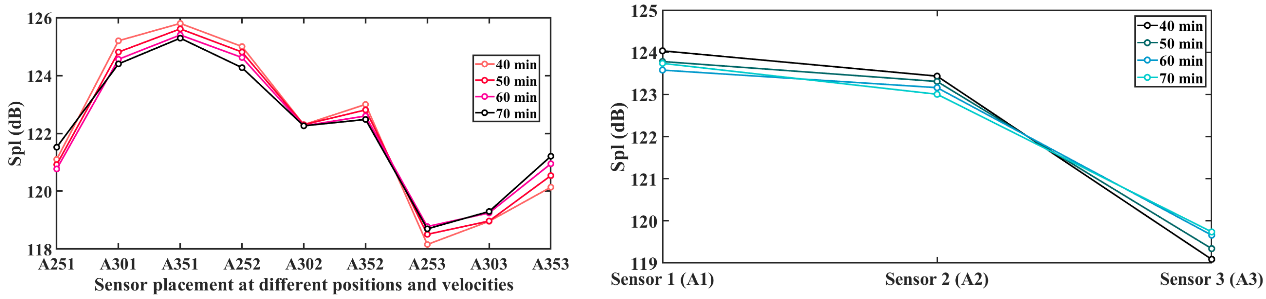

(a) (b)

Fig. 17. (a) Variation in SPL at different sensor positions across various velocities and times, (b) Variation in the average SPL of sensors (with respect to velocity) at different velocities and times.

At the minimum time required to reach the erosion threshold (40 minutes), the signals recorded from the piezoelectrics and the eroded surface area are analyzed. If the SPL calculated from the signals at all velocities is sorted and the corresponding erosion areas are also calculated, the relationship between SPL and the threshold area of the eroded surface can be determined. This relationship, as shown in Fig. 19, is derived using MATLAB Cftools.

$$f(x) = p_1 x^2 + p_2 x + p_3$$
$$p_1 = -0.2842, p_2 = 73.1565, p_3 = -4.6666 \times 10^3 \tag{6}$$

Goodness of fit: SSE: 29.15, R-square: 0.9685, Adjusted R-square: 0.9580.

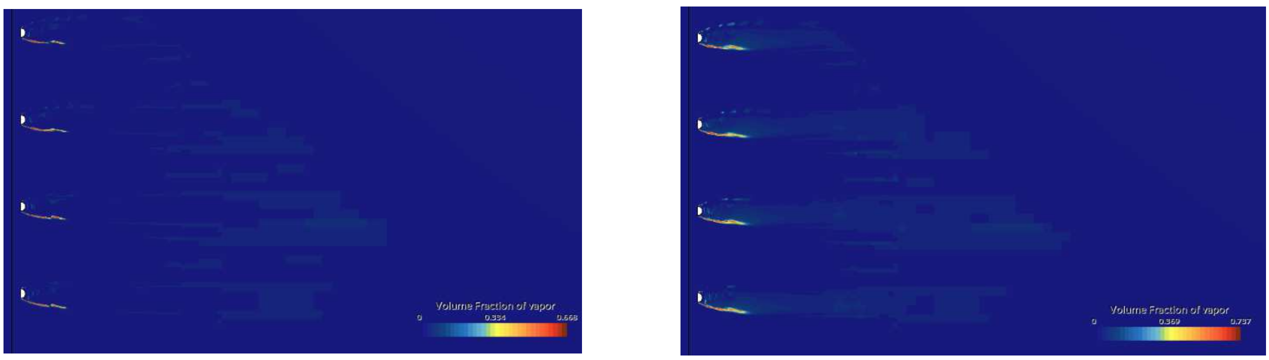

Iteration: 5006 Iteration: 5007

Fig. 18. Volumetric fraction of vapor at an inlet velocity of 3.5 m/s at different times.

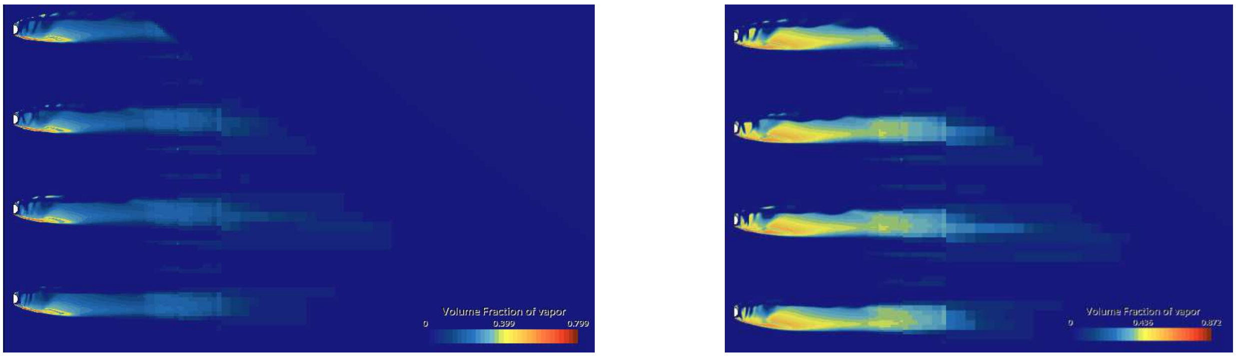

Iteration: 5018 Iteration: 5021

Fig. 18. Continued.

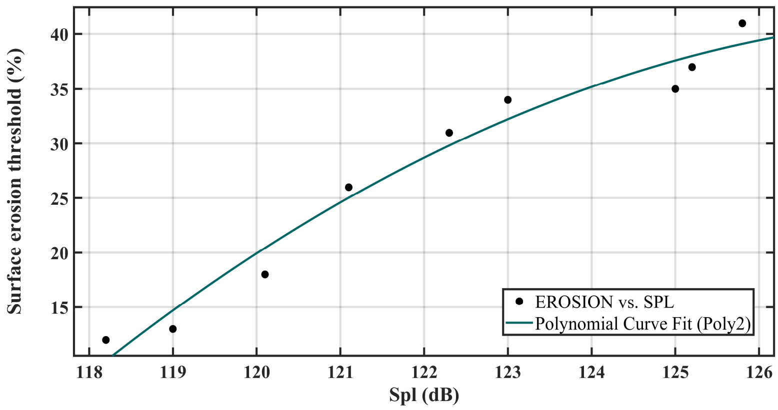

Fig. 19. Relationship between SPL and the threshold area of the eroded surface.

Based on this experiment, to predict the threshold of the eroded levels, a specific number of piezoelectric sensors should be used, depending on the size of the area to be analyzed. If direct installation of the piezoelectric sensor on the surface to be examined is not possible, as in this experiment, the piezoelectric sensor should be installed in a location where the flow pattern over it resembles the flow pattern on the surface of interest. Ultimately, the signals extracted from the piezoelectric sensor are used to calculate the SPL. Cavitation erosion is dependent on the pressure generated by the collapse of bubbles. These pressures are recorded over time using piezoelectric sensors and are then converted to Sound Pressure Level (SPL) using Eq. (4). Given Eq. (6) and knowing the SPL, the threshold area of the eroded surface can be predicted. Thus, for any flow geometry, the pressures generated on the sample are converted to SPL, allowing for the prediction of the eroded surface area. Consequently, this relationship is applicable to any type of flow geometry. This relationship can be general, meaning that if a plate is subjected to a test, even without any color on the plate, whenever the plate reaches the erosion threshold (the time of which is unknown and depends on the material of the sample plate and the fluid flow velocity), the initial area of erosion that could develop on the surface can be predicted based on the extracted SPL.

4. Conclusion

Experimental analysis of cavitation erosion has been rarely and only limitedly conducted. Given that cavitation erosion detection experiments are highly time-consuming, it is possible to predict the eroded surface area of a sample more quickly by establishing a precise pattern and relationship between cavitation acoustics and the eroded surface.

This study focuses on:

- Recording acoustic data from piezoelectrics placed in the test section of a designed channel.
- Developing a precise relationship between these acoustic data and erosion thresholds.
- A novel approach was implemented using an optimized arrangement of piezoelectrics, rather than direct attachment to the sample plate, to capture acoustic signals resulting from cavitation, aided by CFD analysis.
- A semi-cylindrical bluff body was utilized to effectively accelerate cavitation formation.
- Special ink was applied to the surface for faster identification of cavitation erosion:
- A Film Applicator was used to achieve a uniform color with minimal thickness and low adhesion.
- Following a short testing period, signals from the piezoelectrics were recorded and analyzed to calculate the Sound Pressure Level (SPL).
- By computing the SPL and correlating it with a derived formula linking acoustic levels to erosion thresholds, the eroded area of the sample can be predicted.
- A significant aspect of this experimental design is that the relationship between SPL and erosion is independent of the dimensions and geometry of the water tunnel.

This study paves the way for further research into methods for reducing cavitation erosion. For example, the derived relationship can be used to investigate the impact of elastic material properties on reducing erosion on a surface equipped with a cavitation noise absorber, which will be explored in future studies.

Author Contributions

A. Nasseroleslami planned the scheme, initiated the project, and suggested the experiments; conducted the experiments and analyzed the empirical results; A. Sarreshtehdari and M.S. Seif provided the necessary consultations. Additionally, A. Sarreshtehdari, M.S. Seif, and A.A. Ebrahimi Valmoozi facilitated and enabled the use of laboratory equipment and facilities for this project. The manuscript was written through the contribution of all authors. All authors discussed the results, reviewed, and approved the final version of the manuscript.

Acknowledgments

Not applicable.

Conflict of Interest

The authors declared no potential conflicts of interest concerning the research, authorship, and publication of this article.

Funding

The authors received no financial support for the research, authorship, and publication of this article.

Data Availability Statements

The datasets analyzed during the current study are available from the corresponding author on reasonable request.

Nomenclature

d_{33}	Piezoelectric constant [10^{-12} m/V]
ε_r	Relative dielectric constant
ε_0	Vacuum permittivity [Farad/m]
SPL	Sound Pressure Level (dB)
A252	Placement of the piezoelectric element at the middle one-third of the sample plate, with an inlet velocity of 2.5 m/s
A301	Placement of the piezoelectric element at the initial one-third of the sample plate, with an inlet velocity of 3 m/s
A303	Placement of the piezoelectric element at the final one-third of the sample plate, with an inlet velocity of 3 m/s
A352	Placement of the piezoelectric element at the middle one-third of the sample plate, with an inlet velocity of 3.5 m/s
t	Thickness [mm]
$\mathrm{P_{rms}}$	Root mean square pressure
V	Voltage [V]
A251	Placement of the piezoelectric element at the initial one-third of the sample plate, with an inlet velocity of 2.5 m/s
A253	Placement of the piezoelectric element at the final one-third of the sample plate, with an inlet velocity of 2.5 m/s
A302	Placement of the piezoelectric element at the middle one-third of the sample plate, with an inlet velocity of 3 m/s
A351	Placement of the piezoelectric element at the initial one-third of the sample plate, with an inlet velocity of 3.5 m/s
A353	Placement of the piezoelectric element at the final one-third of the sample plate, with an inlet velocity of 3.5 m/s

References

[1] Escaler, X., Farhat, M., Avellan, F., Egusquiza, E., Cavitation Erosion Tests on a 2D Hydrofoil Using Surface-Mounted Obstacles, *Wear*, 254, 2003, 441–9.
[2] Kumar, P., Chatterjee, D., Bakshi, S., Experimental Investigation of Cavitating Structures in the near Wake of a Cylinder, *International Journal of Multiphase Flow*, 89, 2017, 207-217.
[3] Kumar, P., Dhiman, C., Bakshi, S., Numerical Study of Cavitating Structure Near Wake of a Circular Cylinder, *Proceedings of the 10th International Symposium on Cavitation (CAV2018)*, 2019.
[4] Seo, J.H., Moon, Y.J., Shin, B.R., Prediction of Cavitating Flow Noise by Direct Numerical Simulation, *Journal of Computational Physics*, 227, 2008, 6511-6531.
[5] Brandner, P.A., Walker, G.J., Niekamp, P.N., Anderson, B., An Experimental Investigation of Cloud Cavitation about a Sphere, *Journal of Fluid Mechanics*, 656, 2010, 147–76.
[6] Wang, Z., Zhang, M., Kong, D., Huang, B., Wang, G., Wang, C., The Influence of Ventilated Cavitation on Vortex Shedding behind a Bluff Body, *Experimental Thermal and Fluid Science*, 98, 2018, 181-194.
[7] Wu, J., Deijlen, L., Bhatt, A., Ganesh, H., Ceccio, S.L., Cavitation Dynamics and Vortex Shedding in the Wake of a Bluff Body, *Journal of Fluid Mechanics*, 917, 2021, A26.
[8] Yamagata, T., Saito, N., Fujisawa, N., Aeolian Tone from a Semi-Circular Cylinder in a Stream, *Journal of Flow Control, Measurement & Visualization*, 4, 2016, 30-37.
[9] Ghahramani, E., Jahangir, S., Neuhauser, M., Bourgeois, S., Poelma, C., Bensow, R.E., Experimental and Numerical Study of Cavitating Flow around a Surface Mounted Semi-Circular Cylinder, *International Journal of Multiphase Flow*, 124, 2020, 103191.
[10] Escaler, X., Avellan, F., Egusquiza, E., Cavitation Erosion Prediction from Inferred Forces Using Material Resistance Data, *4th International Symposium on Cavitation (CAV2001)*, 2001.
[11] Asnaghi, A., Feymark, A., Bensow, R.E., Computational Analysis of Cavitating Marine Propeller Performance Using OpenFOAM, *Proceedings of the Fourth International Symposium on Marine Propulsors (Smp'15)*, Austin, TX, USA, 2015.
[12] Asnaghi, A., Svennberg, U., Bensow, R.E., Numerical and Experimental Analysis of Cavitation Inception Behaviour for High-Skewed Low-Noise Propellers, *Applied Ocean Research*, 79, 2018, 197-214.
[13] Schenke, S., van Terwisga, T.J.C., An Energy Conservative Method to Predict the Erosive Aggressiveness of Collapsing Cavitating Structures and Cavitating Flows from Numerical Simulations, *International Journal of Multiphase Flow*, 111, 2019, 200-218.
[14] Jahangir, S., Ghahramani, E., Neuhauser, M., Bourgeois, S., Bensow, R.E., Poelma, C., Experimental Investigation of Cavitation-Induced Erosion around a Surface-Mounted Bluff Body, *Wear*, 480-481, 2021, 480-481.
[15] Park, S., Park, J.S., Lee, H., Heo, J., Yoon, Y., Choi, K., Her, N., Ultrasonic Degradation of Endocrine Disrupting Compounds in Seawater and Brackish Water, *Environmental Engineering Research*, 16, 2011, 137-48.
[16] Crum, L.A., Comments on the Evolving Field of Sonochemistry by a Cavitation Physicist, *Ultrasonics Sonochemistry*, 2, 1995, S147–S152.
[17] Usta, O., Sabri, Ç., Korkut, E., An Experimental Study to Investigate Cavitation Noise and Erosion Characteristics, Using Water Jet Test Technique, *Sixth International Symposium on Marine Propulsors Rome*, Italy, 2019.
[18] Han, G., Haosheng, C., Darong, C., Dayun, Y., *Effect of Surface Material on the Cavitation Erosion Noise: Experimental Investigation*, In: Advanced Tribology,

Springer, Berlin, Heidelberg, 2009.
[19] Homa, D., Comparison of Different Mathematical Models of Cavitation, *Transactions of the VŠB - Technical University of Ostrava, Mechanical Series*, 60, 2014.
[20] Varga, J.J., Sebestyen, G., Fay, A., Detection of Cavitation by Acoustic and Vibration-Measurement Methods, *La Houille Blanche*, 1(2), 1969, 137-150.
[21] Ramamurthy, A.S., Bhaskaran, P., Velocity Exponent for Erosion and Noise Due to Cavitation. ASME Pap, 1979.
[22] Kirejczyk, J., Discussion: New Method for Monitoring and Correlating Cavitation Noise to Erosion Capability, *Journal of Fluids Engineering*, 104, 1982, 441–2.
[23] Bull, V., Civale, J., Rivens, I., ter Haar, G., A Comparison of Acoustic Cavitation Detection Thresholds Measured with Piezo-Electric and Fiber-Optic Hydrophone Sensors, *Ultrasound in Medicine and Biology*, 39, 2013, 2406–21.
[24] Rathod, V.T., A Review of Acoustic Impedance Matching Techniques for Piezoelectric Sensors and Transducers, *Sensors (Switzerland)*, 20(14), 2020, 4051.
[25] Tunnel, C., *K23 Cavitation Tunnel*, 2001.
[26] Sipilä, T.P., Sánchez-Caja, A., Siikonen, T.L., Eddy Vorticity in Cavitating Tip Vortices Modelled by Different Turbulence Models Using the Rans Approach, *11th World Congress on Computational Mechanics, WCCM 2014, 5th European Conference on Computational Mechanics, ECCM 2014 and 6th European Conference on Computational Fluid Dynamics*, 2014.
[27] Helal, M.M., Ahmed, T.M., Banawan, A.A., Kotb, M.A., Numerical Prediction of Sheet Cavitation on Marine Propellers Using CFD Simulation with Transition-Sensitive Turbulence Model, *Alexandria Engineering Journal*, 57, 2018, 3805-3815.
[28] Sikirica, A., Carija, Z., Kranjcevic, L., Lucin, I., Grid Type and Turbulence Model Influence on Propeller Characteristics Prediction, *Journal of Marine Science and Engineering*, 7, 2019, 374.
[29] Siemens Digital Industries Software, Simcenter STAR-CCM+ Documentation Version 2021.2, 2021.
[30] Lee, I., Park, S., Seok, W., Rhee, S.H., A Study on the Cavitation Model for the Cavitating Flow Analysis around the Marine Propeller, *Mathematical Problems in Engineering*, 2021(1), 2021, 2423784.
[31] Kamil, K., Amri, A., Rizal, M., Sound Absorption Analysis of Carbon Steel Varied in Density and Microstructures, *INTER-NOISE and NOISE-CON Congress and Conference Proceedings*, 268, 2023, 5434–9.
[32] Brennen, C., *Cavitation and Bubble Dynamics*, Oxford University Press, 1995.
[33] COMSOL Simulation of the Direct Piezoelectric Effect, (n.d.). URL https://www.ultrasonicadvisors.com/comsol-simulation-of-the-direct-piezoelectric-effect, accessed on 27 May 2024.
[34] Mitrovic, D., Zeppelzauer, M., Breiteneder, C., *Features for Content-Based Audio Retrieval, In Advances in Computers*, Academic Press Inc., 2010.
[35] Bell, J.H., Mehta, R.D., Contraction Design for Small Low-Speed Wind Tunnels, *Joint Institute for Aeronautics and Acoustics, (Technical Report) JIAA TR*, 1988.
[36] Murata Manufacturing, *Piezoelectric Ceramic Sensors (PIEZOTITE)*, Ceramics, 2001.

ORCID iD

Ali Sarreshtehdari https://orcid.org/0000-0001-7484-2241

How to cite this article: Nasseroleslami A., Sarreshtehdari A., Seif M.S., Ebrahimi Valmoozi A.A. Experimental Investigation of the Relationship Between Cavitation Acoustic Waves and Erosion Threshold with a Novel Piezoelectric Configuration, *J. Appl. Comput. Mech.*, 11(4), 2025, 1009-1021. https://doi.org/10.22055/jacm.2024.47786.4793